

# Maximum Feedback and Dark Matter Profiles of Dwarf Galaxies

Oleg Y. Gnedin and HongSheng Zhao

*Institute of Astronomy, Cambridge CB3 0HA*

[ognedin@ast.cam.ac.uk](mailto:ognedin@ast.cam.ac.uk), [hsz@ast.cam.ac.uk](mailto:hsz@ast.cam.ac.uk)

## ABSTRACT

The observed rotation curves of dark matter-dominated dwarf galaxies indicate low density cores, contrary to the predictions of CDM models. A possible solution of this problem involves stellar feedback. A strong baryonic wind driven by vigorous star formation can remove a large fraction of the gas, causing the dark matter to expand. We explore the maximum effect of the feedback with an instantaneous removal of the gaseous disk. The energy input depends on the compactness of the disk, hence the specific angular momentum of the disk. For the plausible cosmological parameters and a large range of the disk angular momentum, the feedback is insufficient to destroy the central halo cusp, while the central density is lowered only by a modest factor of 2 to 6. Any realistic modeling of the feedback would have even lesser impact on dark matter. We find that no star formation effect can resolve the problems of CDM cusps.

**Key words:** galaxies: dwarf — galaxies: formation — galaxies: kinematics and dynamics — dark matter

## 1 INTRODUCTION

Dwarf spheroidal galaxies are excellent systems for testing current theories of dark matter. Large mass-to-light ratios indicate that even their centers are dominated by dark matter. The velocity dispersion profile of stars and the rotation curve of gas provide a clean measure of the dynamical mass at all radii. Recent observations of gas-rich dwarfs show a nearly solid-body rotation curve, which implies a finite core inside a few hundred pc (van den Bosch et al. 2000; de Blok et al. 2001). This is in conflict with the predictions of the cold dark matter (CDM) models. Numerical simulations invariably produce a diverging, power-law density “cusp”  $\rho \propto r^{-\gamma}$  with  $\gamma = 1$  (Navarro, Frenk & White 1997) or  $\gamma = 1.5$  (Moore et al. 1999) within  $\sim 500 (M_{\text{vir}}/10^9 M_{\odot})^{1/2}$  pc (Bullock et al. 2001).

The additional disagreements of the CDM models with observations include (1) the prediction of too many dwarf satellites within large halos; (2) the triaxiality of the halos in conflict with almost spherical cores of clusters of galaxies, as inferred from gravitational lensing; (3) the efficient transport of gaseous angular momentum, leading to too small disks of spiral galaxies. Of these, the central cusps seem to be the most severe discrepancy. The CDM models have been very successful in matching observations on scales larger than a Mpc, but these smaller-scale problems have lead to a recent search for the alternatives to CDM. The variants include warm dark matter (e.g., Bode, Ostriker & Turok 2001) and self-interacting dark matter (Spergel & Steinhardt 2000).

We examine an astrophysical solution to the cusp problem, the effect of star formation feedback. The energy released in supernova explosions may heat and ionize the surrounding gas. In the event of an extremely powerful burst of star formation, the heated gas may leave the dwarf galaxy in a form of fast wind. In an idealization of this problem, a significant fraction of the gas may be removed from the dwarf halo on a timescale shorter than the dynamical time. We consider the reaction of the dark matter distribution to the sudden loss of baryonic mass in the center. Supermassive black holes can also have interesting effects, somewhat different from the gas discs, and these will be discussed elsewhere.

## 2 COSMOLOGICAL CONTEXT

We explore the maximum effect of stellar feedback on the dark matter profile, assuming (1) all the gas cooling within the dark halo can be removed; (2) the amount of gas locked in stars is negligible; (3) the removal of gas is instantaneous.

The initial conditions for the dark matter halo and the baryonic disk are set using the cosmological concordance model with  $\Omega_m = 0.35$ ,  $\Omega_\Lambda = 0.65$ ,  $\Omega_b h^2 = 0.02$  (Bahcall et al. 1999), where  $h = 0.65$  is the Hubble constant in units of  $100 \text{ km s}^{-1} \text{ Mpc}^{-1}$ . This gives the average baryon fraction  $f_b \equiv \Omega_b/\Omega_m \approx 0.13$ . Some of the baryons associated with the halo of mass  $M_{\text{vir}}$  will never cool and collapse towards the center, some may be heated and ionized early on and

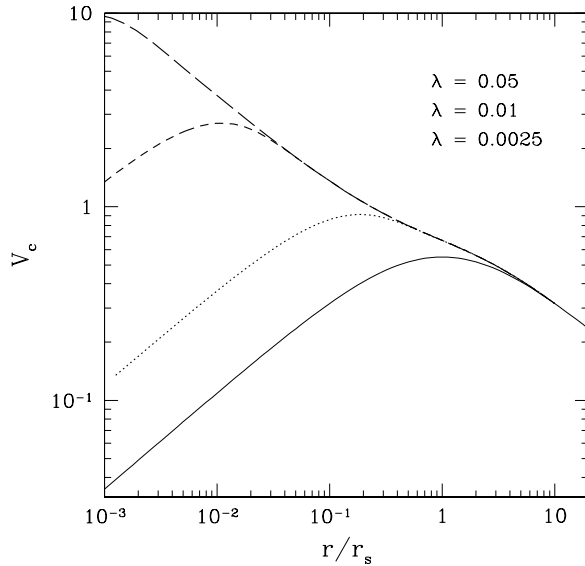


**Figure 1.** Rotation curve before and after the formation of baryonic disk and adiabatic contraction of dark matter, for three values of the angular momentum parameter,  $\lambda = 0.05, 0.01, 0.0025$ .

escape the shallow gravitational well before the starburst. But since we are interested in the maximum effect, we assume that all the associated baryons settle into a disk with the mass  $M_d = f_b M_{\text{vir}}$ .

The size of the rotationally-supported disk,  $r_d$ , is determined by the angular momentum of the baryons. Cosmological simulations show that dark matter halos acquire a log-normal distribution of the dimensionless angular momentum,  $\lambda \equiv J|E|^{1/2}/GM_{\text{vir}}^{5/2}$ , with the mean  $\bar{\lambda} = 0.05$  and dispersion  $\sigma_\lambda = 0.5$ . If the gas had the same angular momentum as the halo, the disk size would scale with  $\lambda$  ( $r_d \sim \lambda^2 r_{\text{vir}}$  if disk is fully self-gravitating, and  $r_d \sim \lambda r_{\text{vir}}$  in the no self-gravity case).

Initially, in isolated halos the gas is supposed to acquire the same angular momentum per unit mass as the dark matter. As a result of hierarchical merging, the distribution of dark matter can become highly non-homogeneous. Also, the cooling and fragmentation of gas into dense clouds can transfer orbital angular momentum to the dark matter via dynamical friction and direct torques. In the end, the gaseous disk may have a significantly lower value of the parameter  $\lambda_b \ll \lambda$ . We mimic the effect of angular momentum redistribution by considering three model disks with different  $\lambda_b$ .

The dark matter distribution self-consistently adjusts to the formation of the disk in the middle of the halo. This process can be described as adiabatic contraction (Flores et al. 1993), which we discuss at length in §3.1. Such condensation of both baryons and dark matter has a significant effect on the central density. Figure 1 demonstrates how adiabatic contraction increases the rotation curve in the inner galaxy over that predicted by cosmological simulations and intensifies the discrepancy with observations.

After the gas blowout, the final distribution of dark matter will depend on the initial disk size in the following

way. If the disk was initially relatively extended ( $r_d \gtrsim r_s$ ) the re-expansion phase is driven by the energy input which is proportional to the binding energy of the disk,  $\propto M_d/r_d$ . If the disk was very compact ( $r_d \ll r_s$ ) only the total removed mass  $M_d$  affects the results. The new equilibrium profile after the removal of the entire baryonic disk must be more extended than that prior to adiabatic contraction, because any rapid expansion increases the actions of dark matter orbits. The faster the expansion, the stronger is the effect.

The energetics of gaseous winds have been studied extensively in the past (Dekel & Silk 1986; van den Bosch et al. 2000 and references therein). In general, dwarf galaxies have shallow potential wells and it is easy to create a strong wind after a few supernova explosions. We shall simply assume that the SNe ejecta energy is sufficient and is efficiently deposited into the gas, to facilitate a rapid expulsion of nearly all the initial baryons with very little locked into stars and stellar remnants.

### 3 ANALYTICAL MODELS

#### 3.1 Two models of adiabatic contraction

We consider the problem in a spherically-symmetric approximation. For the initial virialized halo model we use the Hernquist model, which is a part of the family of models with the mass  $M_{dm}(r_i)$  enclosed within radius  $r_i$  given by

$$\frac{M_{dm}(r_i)}{(1 - f_b)M_{\text{vir}}} = \left( \frac{r_i}{r_s + r_i} \right)^{3-\gamma}, \quad \gamma = 1, \quad (1)$$

where  $r_s$  is the scale radius, and  $\gamma$  is the slope of the cusp. We adopt a concentration parameter  $r_{\text{vir}}/r_s = 10$ , appropriate for dwarf halos at high redshift, but the results at small radii are insensitive to the actual value of this parameter.

During adiabatic contraction, circular orbits conserve angular momentum ( $GM(r)r$ ) and enclosed dark matter mass ( $M_{dm}(r)$ ). An orbit can be labeled interchangeably by its initial radius  $r_i$  or by the specific angular momentum  $j$ , where  $j$  and  $r_i$  are related by

$$j^2 = r_i GM_{dm}(r_i)(1 - f_b)^{-1}. \quad (2)$$

Here we use the constant factor  $(1 - f_b)^{-1}$  to include the mass of baryons assumed to have the same initial distribution. The orbit with an angular momentum  $j$  has a post-contraction radius  $r_j$  given by

$$r_j = \frac{j^2}{GM_{dm}(r_i) + GM_b}, \quad (3)$$

where  $M_b$  is the mass of baryons enclosed within the contracted orbit, which we need to specify separately.

Using observations of disk galaxies as a guide, it is common to assume that the disk would have an exponential surface density profile. The enclosed disk mass  $M_b$  as a function of  $r_j$  is

$$M_{\text{exp}}(r_j) = f_b M_{\text{vir}} [1 - (1 + y) \exp(-y)], \quad y \equiv \frac{r_j}{r_d}, \quad (4)$$

where the scale length  $r_d$  is computed numerically by matching the total angular momentum (e.g., Mo, Mao & White 1998, their eq. 28). In this approach,  $r_j$  is an implicit function of  $r_i$  or  $j$ , and the equation must be solved iteratively.

Here we take a different approach, assuming that the r.h.s. of equation (3) depends on  $r_i$  and  $j$  only, and hence  $r_f$  is computed directly. We note that  $M_b$  is clearly the initial mass of baryons with the specific angular momentum  $< j$ . We postulate that the initial cumulative distribution of the specific angular momentum of both baryons and dark matter is

$$\frac{M_b(< j)}{f_b M_{\text{vir}}} = \frac{M_{dm}(< j)}{(1 - f_b) M_{\text{vir}}} = 1 - \exp\left(-\frac{j^n}{j_0^n}\right), \quad (5)$$

where  $n \equiv (6 - 2\gamma)/(4 - \gamma)$  is a constant defined for a general cusp slope  $\gamma$  of the initial halo. This parametrization is motivated by the fact that in a model with a nearly flat rotation curve,  $j = rv \propto r$ , so that in order to reproduce the final baryon distribution with an exponential profile in  $r_j$  we need a nearly exponential distribution of  $j$ . The characteristic specific angular momentum  $j_0$  is determined by the integrated angular momentum  $J$  of the whole halo,

$$\int_0^\infty dx_j x_j \frac{d}{dx_j} [1 - \exp(-x_j^n)] = \frac{J}{M_{\text{vir}} j_0} = \frac{\lambda GM_{\text{vir}}^{3/2} |E|^{-1/2}}{j_0}, \quad (6)$$

where the l.h.s. can be reduced to the gamma function,  $\Gamma(1 + 1/n)$ . Since the baryons have initially the same distribution as dark matter, the total energy of the system is

$$|E| = (1 - f_b)^{-2} \int_0^\infty dr \frac{dM_{dm}}{dr} \frac{GM_{dm}}{2r} = \frac{GM_{\text{vir}}^2}{4(5 - 2\gamma)r_s}, \quad (7)$$

and we can express  $j_0$  in terms of the  $\lambda$  parameter,

$$j_0 = \frac{\lambda \sqrt{GM_{\text{vir}} r_s}}{\xi}, \quad \xi \equiv \Gamma(1 + 1/n)/\sqrt{4(5 - 2\gamma)}. \quad (8)$$

At small radii the initial mass distribution of dark matter is

$$M_{dm} \rightarrow (1 - f_b) M_{\text{vir}} \left(\frac{r_i}{r_s}\right)^{3-\gamma}, \quad r_i \rightarrow 0, \quad (9)$$

and the initial specific angular momentum

$$j \propto \sqrt{M_{dm} r_i} \propto r_i^{\frac{4-\gamma}{2}} \propto M_{dm}^{\frac{4-\gamma}{6-2\gamma}}. \quad (10)$$

So with our choice of  $n$ , the asymptotic angular momentum distribution of the baryons scales the same way as that of the dark matter:

$$M_{dm} \propto M_b \propto j^n, \quad j \rightarrow 0. \quad (11)$$

It follows then that the mass profiles of the baryons and dark matter are similar before and after the contraction,

$$M_b \propto M_{dm} \propto r_i^{3-\gamma} \propto j^n \propto r_j^{3-\gamma}, \quad (12)$$

where

$$r_j \propto j^{\frac{2}{4-\gamma}} \propto r_i \quad (13)$$

is the post-contraction radius. The contraction factor is finite at small radii, and the cusp slope of the dark matter does not change. To summarize, at small radii after the contraction we have

$$M_{dm} \rightarrow (1 - f_b) M_{\text{vir}} \left(\frac{Cr_j}{r_s}\right)^{3-\gamma}, \quad (14)$$

$$M_b \rightarrow \xi^n \lambda^{-n} f_b M_{\text{vir}} \left(\frac{Cr_j}{r_s}\right)^{3-\gamma}, \quad (15)$$

$$r_j \rightarrow C^{-1} r_i, \quad (16)$$

where

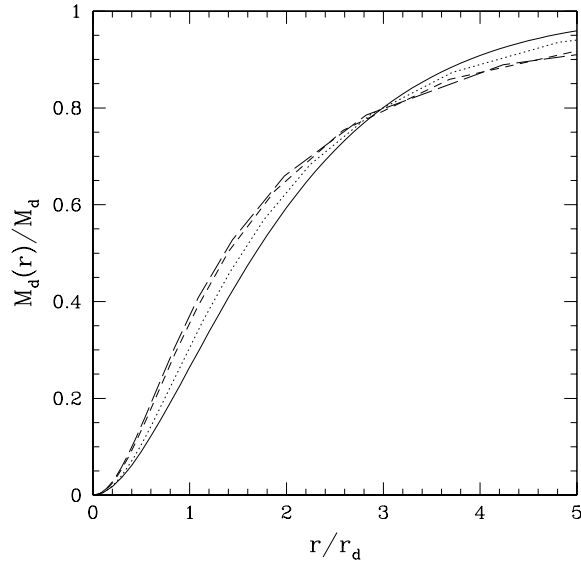


**Figure 2.** Baryon mass profile according to our angular momentum prescription, in comparison with the exponential disk profile (solid line; cf. eq. 4). The radii are normalized to the scale length  $r_d$  computed numerically for three cases:  $\lambda = 0.05$  (dots),  $\lambda = 0.01$  (short dashes),  $\lambda = 0.0025$  (long dashes).

$$C \equiv 1 + (\xi^n \lambda^{-n} - 1) f_b. \quad (17)$$

At a given radius  $r_j$ , the enclosed dark mass and density are enhanced by a factor  $C^{3-\gamma}$ . For an initial Hernquist halo,  $\gamma = 1$ ,  $n = 4/3$ , and  $\xi = 0.265$ . For the disk parameters  $f_b = 0.13$ ,  $\lambda = 0.05 - 0.01$ , the inner dark matter density is enhanced by a factor  $C^2 = 4 - 160$ .

It is interesting to note that the model with  $\gamma = 1$  produces an asymptotic mass distribution at small radii,  $M_b \propto r_j^2$ , similar to that of an exponential disk (cf eq. 4). Figure 2 shows the computed mass profiles of baryons for a family of models with different  $\lambda_b$ . Our analytical models reproduce exponential profiles at 10% level within 0.5–5 scale lengths. The difference in the disk potential is even less and therefore the adiabatic contraction of dark matter is very similar. For all three models, the dark matter profiles computed with the two methods are essentially indistinguishable between  $10^{-3}$  and  $10 r_s$ .

### 3.2 Analytical models of slow wind and fast wind

The expulsion of gas can be worked out analytically in two limiting cases: the adiabatic and instantaneous regimes. We shall refer to these as the slow wind and the fast wind, respectively. The outflow can play a significant role in massive galaxies as well as in dwarf galaxies. Our analytical description is similar to that used in estimating the maximum wind-induced expansion of the dark halo of the Milky Way (Zhao 2001).

To gain more analytical insight, we first consider the slow wind. In this case, a circular orbit of radius  $r_j$  expands to a circular orbit of radius  $r_f$  while conserving the specific angular momentum  $\sqrt{GM(r)}$ . So the expansion factor

is inversely proportional to the combined enclosed mass of baryons and dark matter, i.e.,

$$\frac{r_f}{r_j} \Big|_{\text{slow}} = \frac{M_{dm}(r_j) + M_b(r_j)}{M_{dm}(r_j) + M_b(r_j) - M_{\text{wind}}(r_j)} \quad (18)$$

where  $M_b(r_j)$  and  $M_{dm}(r_j)$  are the baryon and dark matter masses within radius  $r_j$ , and  $M_{\text{wind}}(r_j)$  is the amount of baryons “gone with the wind”. Alternatively, we can write

$$r_f \Big|_{\text{slow}} = \frac{r_j}{1 - f_{\text{wind}}(r_j)}, \quad (19)$$

where

$$f_{\text{wind}}(r_j) \equiv \frac{M_{\text{wind}}(r_j)}{M_{dm}(r_j) + M_b(r_j)}, \quad (20)$$

measures the blown-away mass as a fraction of the dynamical mass. The expansion factor  $r_f/r_j$  is larger in the inner region where the baryons are concentrated and is minimal at the virial radius, where we have only a modest change, since

$$f_{\text{wind}}(r_{\text{vir}}) = \delta f_b \lesssim 0.1, \quad (21)$$

where  $0 \leq \delta \leq 1$  is the total fraction of baryons blown away.

The model for the slow wind can be extrapolated to the fast wind with the following simple formula

$$r_f \Big|_{\text{fast}} = \frac{r_j}{[1 - f_{\text{wind}}(r_j)]^{1+k} (1 - 2\delta f_b)^k}, \quad k \geq 0, \quad (22)$$

where  $k$  and  $\delta$  are adjustable parameters measuring the intensity of the wind in terms of its rapidity and the mass involved, respectively. The slow wind model is recovered for  $k = 0$ , and since we expect a stronger expansion in the fast wind case, we require  $k \geq 0$ . The factor  $1 - 2\delta f_b = 1 - 2f_{\text{wind}}(r_{\text{vir}}) \geq 0$  is motivated by the rule of thumb that a system becomes unbound if it loses half of the mass instantaneously, i.e.,  $r_f \rightarrow \infty$  if  $f_{\text{wind}}(r_{\text{vir}}) = 1/2$  and  $k > 0$ . In a realistic case  $f_{\text{wind}}(r_{\text{vir}}) < 1/2$  and the system remains bound and expands by a certain factor at large radii.

At small radii where the baryons dominate, we can have  $1/2 < f_{\text{wind}}(r_j) < 1$ . In this case the particles at  $r_j$  do not necessarily escape to infinity, because they slow down when they cross outer particles and may still remain bound. We fix the rapidity parameter  $k = \frac{1}{4}$  for the instantaneous wind by matching the results of numerical simulations described in §4. A general wind can be modeled with  $0 \leq k \leq \frac{1}{4}$ .

At very small radii, we have

$$f_{\text{wind}} \rightarrow \xi^n \lambda^{-n} \delta C^{-1} f_b. \quad (23)$$

Combining equations (16,17,22,23), we find that in the center the final post-wind radius  $r_f$  is related to the initial pre-contraction radius  $r_i$  by

$$F \equiv \frac{r_f}{r_i} = \frac{[1 + (\xi^n \lambda^{-n} - 1) f_b]^k}{[1 + (\xi^n \lambda^{-n} (1 - \delta) - 1) f_b]^{1+k} (1 - 2\delta f_b)^k}. \quad (24)$$

The slope of the cusp remains the same. By comparing the dark matter mass within a given radius, we find that the density is reduced by a factor  $F^{3-\gamma}$ .

### 3.3 Maximum effect on the final halo density

The strongest effect on the halo is achieved in the limit of complete removal of the baryonic disk, i.e.,  $\delta \rightarrow 1$ . In this case we have for all radii

$$r_f = \frac{r_i}{(1 - f_b)} \left[ \frac{1 + M_b/M_{dm}}{1 - 2f_b} \right]^k, \quad \delta \rightarrow 1. \quad (25)$$

Interestingly, if the disk forms slowly and is removed slowly as well (i.e., with  $k = 0$ ), the halo expands slightly by a constant factor

$$\frac{r_f}{r_i} = (1 - f_b)^{-1} = \text{const}, \quad (26)$$

as expected from adiabatic invariance. The result is the same if all the baryons were removed from the initial halo distribution without going through the phase of disk formation.

The effect is stronger if a very dense disk ( $\lambda_b \ll 0.05$ ) is removed very fast ( $k > 0$ ). Close to the center, the halo will expand by a factor (cf. eq. 24)

$$F \sim (1 - f_b)^{-1} \left[ \frac{f_b}{(1 - f_b)(1 - 2f_b)} \right]^k \left( \frac{\xi}{\lambda} \right)^{-nk} \sim \left( \frac{0.15}{\lambda} \right)^{\frac{1}{3}}, \quad (27)$$

relative to the original halo model. Here we take  $n = \frac{4}{3}$  and  $\xi = 0.265$  as for the initial Hernquist halo, assume a universal baryon fraction  $f_b = 0.13$  to make a massive disk, and set  $k = 1/4$  for an instantaneous removal of the disk. To summarize, the density of the innermost dark matter can drop at most by a factor  $F^2 = 2 - 6$  for  $\lambda = 0.05 - 0.01$ .

## 4 SPHERICAL SHELL SIMULATIONS

To confirm the analytical results, we compute the dynamics of dark matter using the spherical shell method of Gnedin & Ostriker (1999). The algorithm, originally due to L. Spitzer and collaborators, utilizes the spherical geometry to achieve high resolution in the center. Dark matter particles are distributed on concentric spherical shells at radii  $r_k$  with the mean energy  $E_k$  and angular momentum  $J_k$ . Shells move in the radial direction with velocity  $v_{r,k}$  and can freely cross each other.

We have extended the code by including variable shell masses,  $m_k$ , and improving the corrections for shell crossing. The code solves the equations of motion using the first integral,  $C_k$ :

$$v_{r,k}^2 + \frac{J_k^2}{r_k^2} - \frac{2GM(r_k)}{r_k} = C_k, \quad (28)$$

where  $M(r_k)$  is the mass enclosed within shell  $k$ , including a half of its own mass (accounting for the shell self-gravity):

$$M(r_k) = \sum_{j=1}^{k-1} m_j + \frac{m_k}{2}, \quad (29)$$

if the shells are ordered in radius. The code finds the location of each shell crossing and adjusts the integrals  $C_k$  according to the changed enclosed mass. Because of such corrections, there is no need for force softening and the central region of the system can be probed with very high accuracy. The total energy of the system is conserved exactly, but the individual particle energy accumulates slowly due to the usual numerical relaxation. Further details of the code are described in Gnedin & Ostriker (1999).

In order to investigate the effect of angular momentum loss, we have run three models: Model A with the mean value of  $\lambda = 0.05$ , and Models B and C where  $\lambda$  deviates from its

mean by  $3\sigma_\lambda$  ( $\lambda = 0.01$ , Model B) and  $6\sigma_\lambda$  ( $\lambda = 0.0025$ , Model C).

We use the units  $G = 1$ ,  $M_{\text{vir}} = 1$ ,  $r_s = 1$ , and therefore the results can be scaled to any halo parameters. Each model is run with  $N = 10^4$ ,  $4 \times 10^4$ , and  $10^5$  shells to check numerical convergence. After the disk is removed, the models are run for 40 half-mass dynamical times to achieve new dynamical equilibrium.

Figure 3 shows the initial halo profile and the new equilibrium distribution after the instantaneous removal of the whole disk in Model A. The scale length of the disk,  $r_d = 0.085 r_s$ , is already a fraction of the scale radius of the halo. As expected, there is no change in the profile outside the cusp, at  $r > r_s$ . But even inside the scale radius, the new profile is fairly close to the initial model prior to adiabatic contraction. The central density is affected at most than a factor of 2, in agreement with the analytical prediction (eq. 27).

Figure 4 shows the density profile for Model B. The effect is stronger but there is still no indication of a core forming instead of the cusp. The asymptotic solution increases towards the center as  $r^{-1}$  and describes the numerical distribution reasonably well.

Finally, Model C may have achieved a central core (Figure 5). The inner profile can be fitted with an approximate isothermal sphere,  $\rho \propto (r^2 + r_c^2)^{-1}$ , with  $r_c \approx 0.2 r_s$ . This core radius is significantly larger than the tiny initial scale-length of the disk,  $r_d = 0.00041 r_s$ . However, it seems that the energy input has already saturated in Model C (the change in the binding energy is similar to Model B) and further contraction of the disk would not change the results.

After the disk is removed, the dark matter particles with large enough kinetic energy become unbound. At the end of the simulation, the halo in Model A loses 6.5% of its mass, while the halos B and C lose 14% and 16%, respectively. (About half of those particles becomes unbound during the subsequent evolution of the halo potential towards new equilibrium.) However, as the disk is made progressively more compact, the heating caused by disk removal is shared by a small number of particles in the center. They reach very high velocity and leave the system, but most of the particles remain unaffected. In the limit of an infinitely small disk, the final equilibrium profile would be close to our extreme Model C.

Navarro, Eke & Frenk (1996) studied the effect of instantaneous disk removal using a three-dimensional N-body code. They also used a Hernquist model for the initial dark matter profile and imposed an external potential of the exponential disk. Instead of analytically calculating the adiabatic contraction, they let the dark matter halo to adjust dynamically to the disk potential. Then, they remove the disk and study the subsequent expansion of the halo. Navarro et al. find that the core does develop in the inner regions of all of their models. They fit a non-singular isothermal sphere to the inner 25% of the mass and find the core radii satisfying the following relation:  $r_c = 0.11 (M_d/r_d)^{1/2} r_s$ , where  $M_d$  is the mass of the disk in units of the halo mass (or  $f_b/(1-f_b)$ , in our notation).

The expansion effect that Navarro et al. find is much stronger than our simulations or analytical calculations show. For example, their fit for the core radius for our Model C would give  $r_c \approx 2.1$ , about ten times the value we find. In

Models A and B the core radii should also have been easily detectable, according to the fit.

We identify two possible reasons for the disagreement, force resolution and numerical relaxation effects. Firstly, a force softening at  $0.03 r_s$ , used by Navarro, Eke & Frenk (1996), prevents an accurate calculation of the dynamics of inner shells, especially in cases of very small disks. This would naturally cause a development of a core in the particle distribution, although the core radii found by Navarro et al. are larger than the softening length. Secondly, numerical effects must be important, as their simulations use only  $N = 10^4$  particles. Two-body scattering of the particles (or, numerical relaxation) may significantly alter the density profile on a timescale  $t_r \sim 0.1 N / \ln N \sim 100$  time units. This is a few times shorter than the duration of Navarro et al. experiments. Finally, we note that even though the numerical profile before disk removal may be stable, as Navarro et al. show, having a small number of particles left in the center afterwards would lead to a simple statistical undersampling of the density distribution, posing as a 'core'. This is similar to the issue of resolving central cusps in cosmological simulations: higher resolution runs converge to a steeper profile.

It is likely that the difference in the results is not related to 1D vs 3D simulations. In our one-dimensional models, all shells conserve their initial angular momentum and do not experience any non-radial perturbations. But since the dark matter halo is not centrifugally supported, conservation of angular momentum should not seriously affect the dynamics. Also, the remaining stellar distribution in dwarf spheroidal galaxies is observed to be roughly spherical, so we can expect the dark matter halo to be spherical as well, lending support to our 1D models.

Note, that our simulations achieve much higher resolution, with ten times more particles and no force softening in the center. But the statistical error-bars in Figure 5, proportional to the square root of the number of particles in the bin, show that even our models cannot probe regions smaller than  $0.01 - 0.03 r_s$ . At larger radii, except for the extreme model C, we do not find any significant flattening of the dark matter distribution.

Our results demonstrate that stellar feedback is insufficient to reduce the central dark matter density. We illustrate this point for a prototypical low density dwarf galaxy DDO 154. Figure 6 shows the observed rotation curve of DDO 154, which peaks at  $48 \text{ km s}^{-1}$ . As this is perhaps the most robustly determined quantity, we normalize the simulation results to have the same value and location of the circular velocity. The simulated curves correspond to the equilibrium density profiles of Models A, B, and C (Figures 3–5). They are clearly more concentrated than allowed by the data.

In addition, the scale radii of the initial halo in Figure 6 increase as the effect of feedback gets weaker (corresponding to the larger disk). For Model C  $r_s = 2.9 \text{ kpc}$ , but for the less perturbed models B and A it is  $r_s = 3.6$  and  $5.6 \text{ kpc}$ , respectively. The virial halo mass is about the same, around  $1.2 - 1.3 \times 10^{10} M_\odot$ . This mass is lower than the best-fitting value ( $\sim 3 \times 10^{10} M_\odot$ ) from van den Bosch et al. (2000), and yet the resulting rotation curve is well above observations.

Note that we do not attempt any accurate fitting of the rotation curve, which would require taking into account beam-smearing effects. However, in case of DDO 154 the beam size is less than 1 kpc van den Bosch et al. (2000) and

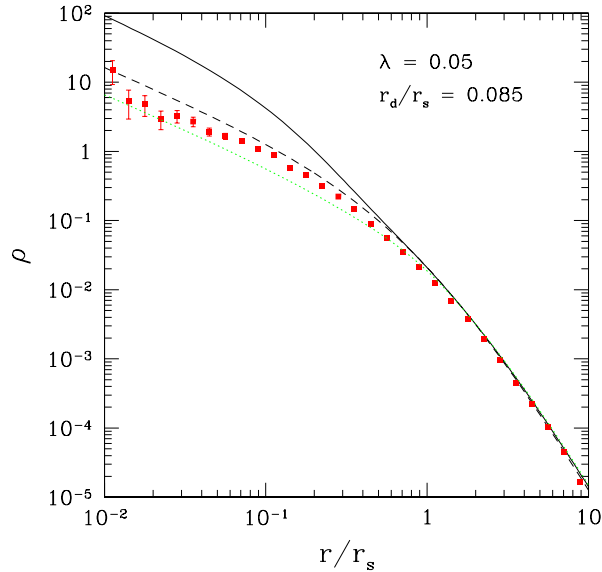


**Figure 3.** Density profile for Model A ( $\lambda = 0.05$ ,  $f_b = 0.13$ ,  $\delta = 1$ ) at the end of simulation with  $10^5$  shells. Dashed line is the initial Hernquist model, solid line is the halo profile after adiabatic contraction. Symbols show the results of numerical simulations for a new equilibrium profile after the removal of the baryonic disk. Errorbars are the sampling uncertainty. Dotted line is the analytical prediction, eq. (22).

therefore the qualitative disagreement with the data would remain.

## 5 SUMMARY

We have explored the effect of maximum feedback on the central density of dark matter halos of gas-rich dwarfs, combining analytical limits with numerical simulations. The expansion of dark matter after the removal of the entire disk is controlled by the mass and compactness of the disk. For a wide range of the baryon angular momentum, we find the effect to be modest, at most a factor of a few reduction in the central halo density. This is hardly enough to bring the models into agreement with the observed solid-body rotation curves, as we demonstrate for the case of DDO 154.

We conclude that the slowly rising rotation curves are likely to be a genuine problem of CDM models. It might be necessary to consider other possible solutions, such as the effect of merging of massive black holes or an unusual property of dark matter particles.

## REFERENCES

Bahcall N. A., Ostriker J. P., Perlmutter S., Steinhardt P. J., 1999, *Science*, 284, 1481  
 Bode P., Ostriker J. P., Turok N., 2001, [astro-ph/0010389](#)  
 Bullock J. S. et al. 2001, *MNRAS*, 342, 559  
 Carignan C., Beaulieu S., 1989, *ApJ*, 347, 760  
 de Blok W. J. G., McGaugh S. S., Bosma A., Rubin V. C., 2001, *ApJ*, 552, L23

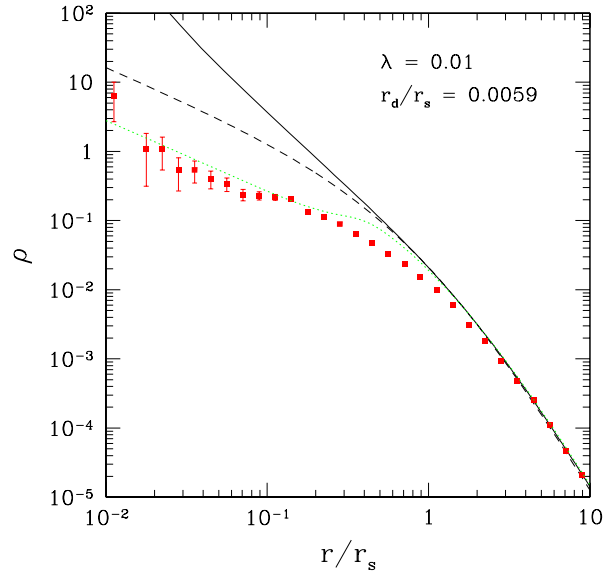


**Figure 4.** Density profile for Model B ( $\lambda = 0.01$ ). Lines are as in Figure 3.

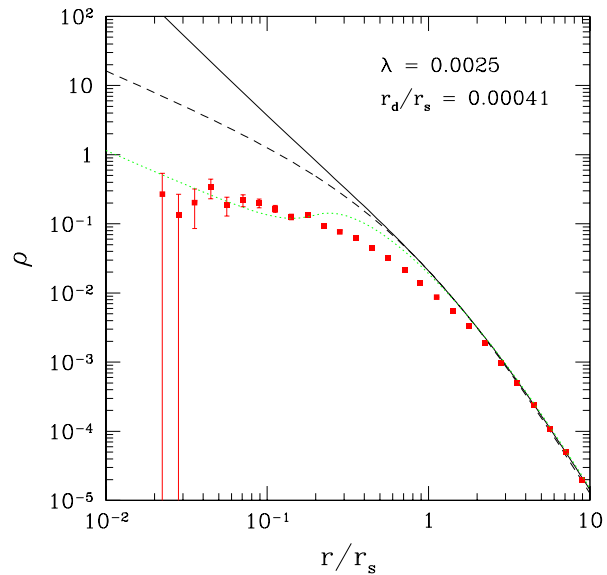


**Figure 5.** Density profile for Model C ( $\lambda = 0.0025$ ). Lines are as in Figure 3.

Dekel A., Silk J., 1986, *ApJ*, 303, 39  
 Flores R., Primack J. R., Blumenthal G. R., Faber S. M., 1993, *ApJ*, 412, 443  
 Gnedin O. Y., Ostriker J. P., 1999, *ApJ*, 513, 626  
 Mo H. J., Mao S., White S. D. M., 1998, *MNRAS*, 295, 319  
 Moore B., Quinn T., Governato F., Stadel J., Lake G., 1999, *MNRAS*, 310, 1147  
 Navarro J. F., Eke V. R., Frenk C. S., 1996, *MNRAS*, 283, L72  
 Navarro J. F., Frenk C. S., White S. D. M., 1997, *ApJ*, 490,

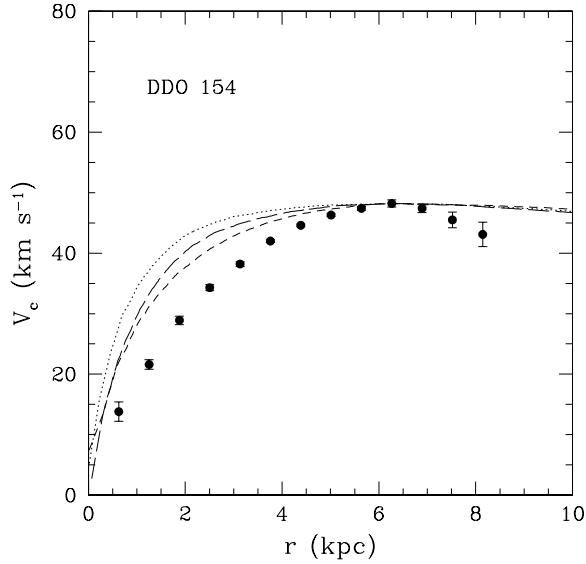


**Figure 6.** Rotation curve of DDO 154 from a high-resolution HI data (from Carignan & Beaulieu 1989) vs final circular velocities of Models A (dots), B (short dashes), and C (long dashes). The simulated rotation curves are normalized to pass through the maximum of the observed one, with no formal fitting attempted.

493  
 Spergel D. N., Steinhardt P. J., 2000, Phys. Rev. Lett., 84,  
 3760  
 van den Bosch F. C., Robertson B. E., Dalcanton J. J., de  
 Blok W. J. G., 2000, AJ, 119, 1579  
 Zhao H.S. 2001, in preparation